

## Fibers and cylinders of cryptomelane-hollandite in Permian bedded salt, Palo Duro Basin, Texas

HARVEY E. BELKIN, E. LAURENCE LIBELO\*

959 National Center, U.S. Geological Survey, Reston, Virginia 22092, U.S.A.

### ABSTRACT

Fibers and thin-walled, hollow cylinders of cryptomelane-hollandite have been found in both the chevron and the clear salt from various drill cores in Permian bedded salt from the Palo Duro Basin, Texas. We have examined selected core sections from the lower San Andres (units 3, 4, 5), upper San Andres, lower Clear Fork, and the Salado-Tansill Formations. We have found fibers or cylinders from only the lower San Andres Formation units 4 and 5, the upper San Andres Formation, and the Salado-Tansill salt. The fibers are inorganic, light to dark reddish brown, pleochroic, highly birefringent, filamentary single crystals, <1 to ~5  $\mu\text{m}$  in diameter, with length-to-diameter ratios of at least 20:1 (some > 5000:1). Energy-dispersive analyses (SEM) and Gandolfi X-ray diffraction techniques have identified the fibers and cylinders as members of the cryptomelane-hollandite series. Tunnel cations (A) of the model composition  $\text{A}_{0-2}(\text{Mn}^{2+}, \text{Mn}^{3+})_8(\text{O}, \text{OH})_{16}$  were found to be  $\text{K}^+$  and  $\text{Ba}^{2+}$ . Pure (within the limits of the technique)  $\text{K}^+$  and  $\text{Ba}^{2+}$  end members as well as intermediate compositions were observed.

The fibers can be straight and/or curved, can bifurcate, can form loops, waves or spirals, and can be isolated or in parallel groups. Detailed petrographic analyses show no evidence for recrystallization or deformation of the enclosing salt after fiber formation. Many fibers appear to radiate from a point, line, or planar source. Although our observations do not provide a definitive explanation for fiber origin, we suggest that the fibers grew in situ by a solid-state diffusional process at low temperatures.

The cylinders are pleochroic, highly birefringent, light to dark reddish brown, hollow, thin-walled, open-ended right cylinders, having a 1- to 2- $\mu\text{m}$  wall thickness and variable lengths (2 to 434  $\mu\text{m}$ ) and diameters (6 to 55  $\mu\text{m}$ ). There also appear to be single crystals of cryptomelane-hollandite, but these are found almost entirely in fluid inclusions in the chevron and clear salt. Their presence in the primary halite suggests that they were formed contemporaneously with the chevron structure and were accidentally trapped in the fluid inclusions. The cylinders found in the recrystallized salt are perhaps a residue from dissolved chevron salt.

The observation of cylinders partially or completely enclosed by salt stratigraphically above large fluid inclusions suggests that natural downward fluid-inclusion migration has occurred, in response to the geothermal gradient.

### INTRODUCTION

The safe, long-term storage of nuclear wastes is a problem of considerable importance. Underground sites in bedded salt are being considered from both a socio-political and scientific standpoint (e.g., McClain and Russell, 1980; Roedder and Bassett, 1981). During a detailed fluid-inclusion and petrographic study of the halite-rich cores from bedded salt deposits of the Palo Duro Basin, Texas, as part of the site-selection process under contract with the University of Texas at Austin, Bureau of Economic Geology, we discovered an unusual occurrence of

cylinders and fibers of the cryptomelane-hollandite series. Cylinders and fibers have been found in the studied core from both the Salado-Tansill salt, the lower San Andres units 4 and 5, and the upper San Andres in the Permian Palo Duro Basin. The cylinders appear to be related to both primary halite precipitation and subsequent halite recrystallization. They always occur in or very near fluid inclusions. The fibers, however, are not obviously related to fluid inclusions. The fibers occur enclosed in primary chevron salt and in recrystallized halite and also transect both types.

In this paper we describe the petrography of the cryptomelane-hollandite cylinders and fibers in relation to the various salt types. Although we do not completely understand the origin of these features, we present some possible modes of origin. The cylinders and fibers may

\* Present address: Civil Engineering Department, Virginia Polytechnic Institute and State University, Blacksburg, Virginia 24061, U.S.A.

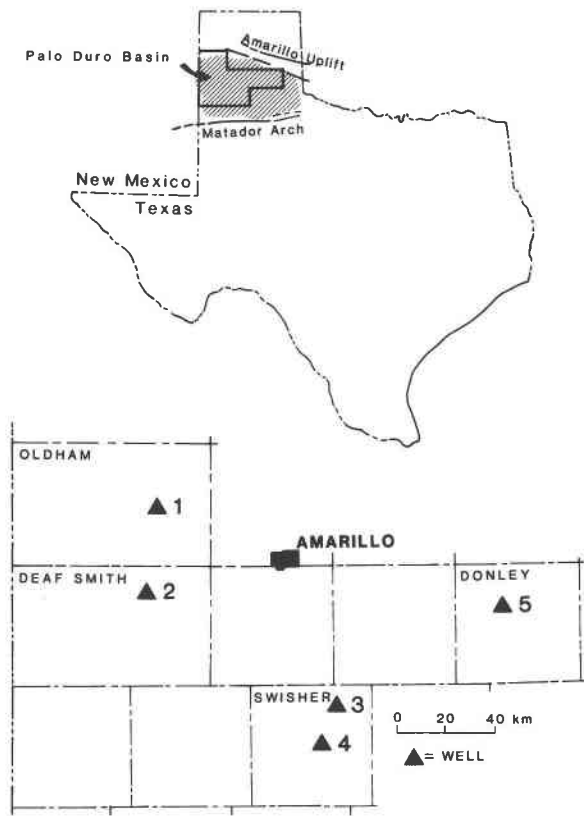


Fig. 1. Index map showing the location of the Palo Duro Basin in the Texas panhandle, bordered on the north by the Amarillo uplift and on the south by the Matador arch. The enlarged insert shows the location of the five studied wells in the vicinity of Amarillo, Texas. 1 = Oldham County, Stone & Webster Engineering Corp. No. 1 Mansfield; 2 = Deaf Smith County, Stone & Webster Engineering Corp. No. 1 J. Friemel (Wildcat); 3 = Swisher County, D.O.E., Gruy Federal, Inc. No. 1 Grabbe; 4 = Swisher County, Stone & Webster Engineering Corp. No. 1 Zeeck; 5 = Donley County, Stone & Webster Engineering Corp. No. 1 Sawyer.

provide information on conditions of original halite deposition and subsequent recrystallization.

#### GEOLOGIC SETTING AND DEPOSITIONAL ENVIRONMENT

All the studied samples were from cores drilled through the Permian evaporite sequence of the Palo Duro Basin, Texas (Fig. 1). The Palo Duro Basin lies in the central portion of a larger Permian Basin defined by that area underlain by bedded salt deposits (Johnson and Gonzalus, 1978). Overlying the igneous and metamorphic basement are thin and discontinuous Cambrian(?) and Ordovician sandstones and carbonates. Several hundred feet (1 ft = 0.3048 m) of Mississippian limestone and dolostone locally interbedded with shale and sandstone follow and are covered by Pennsylvanian arkosic sandstones, shales, and limestones.

The Permian section in the Palo Duro Basin contains the strata studied. Six major salt beds occur in the Leo-

nardian, Guadalupian, and Ochoan rocks. The Leonardian Series, ~610 m thick, is composed of dolostones, shales, anhydrites, siltstones, and salt. The lower Clear Fork Formation within the Leonardian Series, is typically over 125 m thick and consists of dolostone, anhydrite, shale, and salt. It is the oldest Permian unit to contain cyclic evaporites and represents deposition of two offlapping evaporite cycles principally within a coastal sabkha salt-pan environment (Dutton et al., 1979; Handford, 1981). Lower and upper divisions of the San Andres Formation (Leonardian and Guadalupian Series) have been established by the Texas Bureau of Economic Geology (Presley, 1980) with five subdivisions of the lower San Andres based on depositional cycles (units 1, 2, 3, 4, 5; Hovorka, 1983; Fracasso and Hovorka, 1986). Each cycle starts with a thin black mudstone and continues through limestone, dolostone, nodular anhydrite, laminated anhydrite, and massive bedded halite and ends with chaotic mixtures of halite and mudstone. This sequence represents deposition progressing from a lower sabkha environment to a transgressive upper sabkha salt environment, located in the northern part of the Palo Duro Basin.

The salt in the Salado (early Ochoan) and Tansill (late Guadalupian) Formations occurs as a single massive sequence (hence, called the Salado-Tansill salt) with interbedded shale and represents upper sabkha deposition (Dutton et al., 1979).

Various detailed studies of the Permian salt-bearing strata (siliciclastic facies, salt, anhydrite, and dolostone) suggest that these rocks generally reflect deposition in restricted, inner-marine shelf and coastal sabkha environments (Dutton et al., 1979). Sabkhas and associated brine pools are shallow environments susceptible to periodic influx of terrestrial or marine-derived fluids. Although a deep basin model has been argued for some evaporite deposits (Schmalz, 1969), common features observed in salt in the Palo Duro Basin, such as vertically oriented halite crystals with chevron zones (Fig. 2), are also observed in modern sediments forming by bottom-nucleated growth in shallow brine pools (Arthurton, 1973; Shearman, 1978). Roedder (1982) has argued for shallow water as a necessary condition for the formation of the chevron pattern. The halite also shows dissolution textures that suggest that periodic brine-pool desiccation resulted in prolonged episodes of subaerial exposure (Hovorka, 1983; Fracasso and Hovorka, 1986). Recently, Hovorka (1985) also has argued that sabkha, salina, playa, or deep-water basin models should not be used to describe the depositional environment of the San Andres Formation. She has suggested that the lithology indicates that the shallow-marine shelf environment of the San Andres underwent intermittent subaerial exposure between episodes of flooding with marine brines.

#### STUDIED SAMPLES

All the samples were pieces of oriented drill core (Fig. 1) supplied by the Bureau of Economic Geology, Uni-

TABLE 1. Distribution of fibers and cylinders in the studied Palo Duro Basin core samples

Well	Core interval (ft)*	Formation	Fibers	Cylinders
Stone & Webster Engineering Corp., No. 1 Mansfield (Oldham County)	1543.0–1543.3	unit 4†	0	0
	1589.7–1590.2	unit 4†	X	0
	1608.0–1608.7	unit 4†	X	0
	1622.6–1623.1	unit 4†	X	X
	1638.6–1639.0	unit 4†	X	X
	1685.4–1686.0	unit 4†	X	X
	1690.8–1691.3	unit 4†	X	X
D.O.E. Gruy Federal, Inc., No. 1 Grabbe (Swisher County)	1041.7–1042.3	Salado-Tansill	0	0
	1050.5–1050.7	Salado-Tansill	0	0
	1056.2–1056.8	Salado-Tansill	X	0
Stone & Webster Engineering Corp., No. 1 Sawyer (Donley County)	838.3–838.8	unit 3†	0	0
	839.5–839.7	unit 3†	0	0
	1995.8–1996.2	lower Clear Fork	0	0
Stone & Webster Engineering Corp., No. 1 J. Friemel (Wildcat) (Deaf Smith County)	2401.5–2401.8	unit 5†	0	0
	2409.9–2410.3	unit 5†	X	X
	2580.7–2581.1	unit 4†	0	0
	2594.7–2595.1	unit 4†	0	0
	2616.2–2616.6	unit 4†	X	0
	2625.0–2625.3	unit 4†	0	0
	2634.1–2634.4	unit 4†	0	0
	2634.6–2634.9	unit 4†	0	0
	2642.9–2643.2	unit 4†	X	X
	2644.9–2645.2	unit 4†	X	0
	2660.2–2660.5	unit 4†	0	0
	2671.7–2671.9	unit 4†	0	0
	2682.9–2683.3	unit 4†	0	0
2728.8–2729.1	unit 4†	0	0	
Stone & Webster Engineering Corp., No. 1 Zeeck (Swisher County)	2149.3–2149.7	upper San Andres	X	X

Note: X = presence of fibers of cylinders; 0 = not found.  
\* For conversion, 1 ft = 0.3048 m.  
† Lower San Andres.

versity of Texas at Austin, especially for a fluid-inclusion study of the halite (Roedder et al., 1987). Table 1 shows the core interval, well identification, stratigraphic unit, and location.

#### CRYPTOMELANE-HOLLANDITE SERIES

Cryptomelane and hollandite form a series with the general formula  $A_{0-2}(Mn^{4+}, Mn^{3+})_8(O, OH)_{16}$ , where A is primarily  $Ba^{2+}$  in hollandite and  $K^+$  in cryptomelane (Post et al., 1982). Fleischer (1983) gave a similar formula but replaced  $Mn^{3+}$  with  $Mn^{2+}$ . The minerals are monoclinic with pseudotetragonal symmetry. The name *cryptomelane* was proposed by Richmond and Fleischer (1942) for a distinct mineral species that had been included in the general category "psilomelane." Fleischer and Richmond (1943) showed that hollandite is related to and isostructural with cryptomelane.

A fiber habit is very common in manganese oxide minerals (e.g., Radcliffe, 1974; Finkelman et al., 1974; Frenzel, 1980). However, we know of no reported description of cryptomelane-hollandite cylinders.

#### CRYPTOMELANE-HOLLANDITE IN SALT AND OTHER OCCURRENCES

Although cryptomelane-hollandite is a relatively common mineral usually associated with weathering and hy-

drothermal deposits (Potter and Rossman, 1979; Frenzel, 1980; Hewett and Fleischer, 1960), we have found only one mention of cryptomelane-hollandite in salt deposits. Sun (1962) describes oriented intergrowths of cryptomelane in sylvite from Carlsbad, New Mexico. They occur in the Salado Formation in the Delaware Basin, west of the Palo Duro Basin. Sun (1962) described and showed in three photomicrographs a fiber density seen only occasionally in salt from the Palo Duro Basin. He also described features similar to those of cryptomelane-hollandite from the Palo Duro Basin such as fiber bifurcation, random and crystallographically controlled orientations, and a similar fiber size.

#### OPTICAL PROPERTIES

Although we did not determine index of refraction or optical sign we describe below other optical properties that were easily obtained without removing the fibers or cylinders from the host halite. The color, in plane-polarized transmitted light, of both the fibers and cylinders varied from light to dark reddish brown. The cylinders and fibers are also pleochroic from light to dark reddish brown. Most of the fibers appear black because of total reflection due to the large difference in refractive index between halite ( $n = 1.54$ ) and the cryptomelane-hollandite series ( $n > 2.90$ ). Where observed, all the fibers had

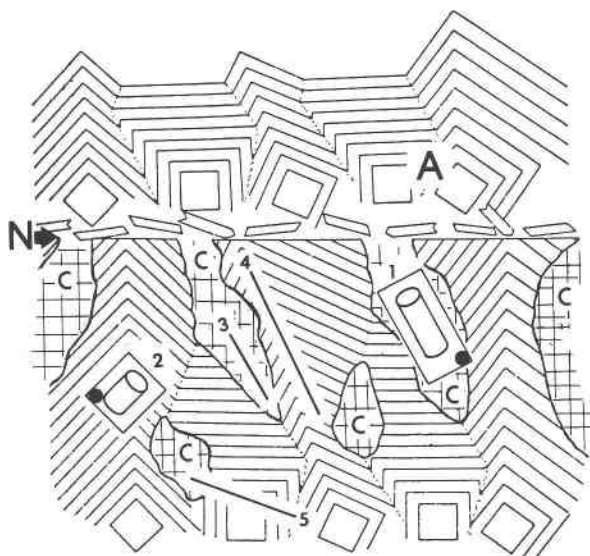


Fig. 2. Schematic diagram showing a typical layered halite sequence resulting from foundered hopper rafts, followed by competitive growth and dissolution and precipitation. The typical locations of the cryptomelane-hollandite cylinders and fibers are also shown. A = zone of foundered hopper crystals; those whose apices are directed upward have grown into a chevron pattern. N = the truncated surface caused by dissolution; this is the site for additional nucleation and accumulation of hopper crystals. Clear halite (C) occurs throughout the layered sequence. Features include (1) a fluid inclusion in clear salt containing a cylinder, (2) a fluid inclusion in massive chevron salt containing a cylinder, (3) a fiber completely contained in clear halite, (4) a fiber completely contained in massive chevron salt, and (5) a fiber that transects both the clear and chevron halite. Modified from Shearman (1978).

parallel extinction and positive elongation (length-slow). The cylinders had parallel extinction when viewed perpendicular to their axes of revolution and negative elongation (length-fast) parallel to their axes of revolution. An estimate of the fiber and cylinder birefringence using the interference color chart of Kerr (1959) is  $b > 0.26$ .

#### X-RAY DIFFRACTION AND ENERGY-DISPERSIVE ANALYSIS

The small size and volume of the fibers ( $\sim 1\text{--}3\ \mu\text{m}$  in diameter) required the use of the Gandolfi camera technique (Gandolfi, 1967; Zolensky and Bodnar, 1982). Pieces of halite containing numerous fibers were isolated from the surrounding barren halite by selective cleaving. The halite piece was then dissolved in water and the fibers concentrated. After washing the fibers thoroughly, they were attached to a glass fiber. The samples were run at 40 kV and 30 mA with Ni-filtered Cu radiation. Runs of 6 to 24 h were successful. Twelve runs produced usable patterns. All patterns were similar, but some produced more lines than others. The  $d$  spacings matched the values given for cryptomelane (Table 2). A cylinder from No. 1 J. Friemel 2642.9–2643.2 (see Table 1) was ex-

TABLE 2. Observed and calculated X-ray powder-diffraction data

$d_{\text{calc}}$ (Å)	$I_{\text{calc}}$	$hkl$	$d_{\text{obs}}$ (Å)	$I_{\text{obs}}^*$
6.94	26	110	7.01	m
4.908	32	200	4.91	w
3.470	11	220	3.49	w
3.104	68	310	3.06	m
2.734	1	101		
2.454	7	400		
2.389	100	211	2.39	s
2.313	3	330	2.31	m
2.195	7	420	2.21	w
2.148	18	301	2.16	s
1.9249	4	510		
1.8262	12	411	1.83	s
1.7351	1	440	1.73	w
1.6833	2	530		
1.6358	12	600	1.63	w
1.6161	5	431		
1.5519	1	620		
1.5350	9	521	1.54	m
1.4235	5	002	1.43	w
1.4038	1	611		
1.3881	1	550		
1.3671	1	202		
1.3611	1	640		
1.3497	2	541	1.35	w
1.3170	1	222		
1.3013	2	631	1.30	w
1.2939	4	312		

Note: Calculated data from JCPDS no. 29-1020, a pure  $\text{K}^+$  cryptomelane; observed data = an average of four samples.

\* Intensities estimated visually; s = strong, m = medium, w = weak.

amined by TEM diffraction techniques and was found to have a cryptomelane-hollandite structure (Barbara Miner, pers. comm.).

Both fibers and cylinders were successfully prepared for energy-dispersive X-ray analysis by SEM. The predominant spectrum observed contained Mn, K, and Ba, generally with  $\text{K} > \text{Ba}$ . However, in some cases Ba was absent, and in one case K was absent. Our data are too limited to show any correlation with depth or formation.

This combination of techniques indicates that the cylinders and fibers are members of the cryptomelane-hollandite series  $(\text{K}, \text{Ba})(\text{Mn}^{4+}, \text{Mn}^{3+})_8(\text{O}, \text{OH})_{16}$ . All the fibers, cylinders, and other shapes observed in the salt appear to have similar optical properties; thus, we assume that they are all members of the cryptomelane-hollandite series.

#### PETROGRAPHY

The initial petrography was done on thick (2–3 mm) polished plates. Additional study usually involved cleaving small pieces with a sharp edge. Sample preparation was designed so that the salt always remained at ambient temperature.

#### Salt

Before describing the features of the fibers and cylinders, it is useful to discuss the kinds of bedded salt. We distinguish two kinds: (1) chevron salt and (2) clear salt.

Hopper crystals are formed by evaporation on a calm

surface of a super-saturated brine. Nucleation at the air-brine interface produces thin tablets, usually with a depressed center (hopper) that are suspended by surface tension on the air-brine interface. The hopper crystals tend to accumulate to form rafts and eventually sink (Shearman, 1978). During the hopper growth, numerous small fluid inclusions tend to be trapped and outline the cubic growth faces (Roedder, 1984). Growth, however, can continue even when the hopper rafts lie on the bottom of the basin. Salt grows fastest in the [111] direction. Shearman (1978) suggests that competitive growth between variously oriented nuclei will favor those with cube corners (body diagonals) oriented vertically and hence pointed toward the source of new material. The growth stages of these bottom-growing crystals are also outlined by numerous small fluid inclusions parallel to the cube faces. A vertical section through such salt will show a chevron-like pattern of planes of fluid inclusions (Fig. 2). Both hopper crystals and the subsequent chevron salt are primary depositional features of the bedded evaporite. However, we only recognize this salt by the alternation of fluid inclusion-rich lamellae with clear lamellae (Fig. 2, Fig. 7H). Inclusion-free, clear salt that formed simultaneously with the chevron salt would not be recognized as such.

Clear salt is characterized by large crystals ( $\sim 1$  cm) and few but large ( $> 100 \mu\text{m}$  on an edge) fluid inclusions. A very common feature in bedded salts (Shearman, 1978) is voluminous clear salt filling obvious dissolution channels in the original chevron salt framework. Roedder (1984) has defined two types of clear salt: (1) that produced by crystallization processes on the bottom of the basin and (2) that produced by recrystallization processes at some later time and, hence, distinct from the primary depositional environment. The petrographic distinction between these two types is difficult (Roedder, 1984). Roedder et al. (1987) have chemically analyzed large, individual fluid inclusions from the clear salt of the Palo Duro Basin. They found a very large intersample and intrasample chemical variation that indicates that the clear salt is polygenetic. Roedder et al. (1987) have suggested that the diversity in composition of fluid inclusions in clear salt may originate from the combination of a variety of sources for the clear salt-forming fluids (e.g., Permian sea, meteoric, and ground water as well as later migrating fluids).

### Fiber morphology

The cryptomelane-hollandite fibers are filamentary single crystals with small cross-sectional areas, usually  $\sim 10 \mu\text{m}^2$ , and with length-to-diameter ratios greater than 20. The fibers appear similar to "whiskers" (Figs. 3A, 3B) described by materials scientists (e.g., Shaffer, 1967; Evans, 1972; Ahmad, 1970). These are usually very strong and are also characterized by essentially no growth on the whisker sides. The supersaturation of the side faces of the cryptomelane-hollandite fibers must also have been sufficiently low to prevent two-dimensional nucleation.

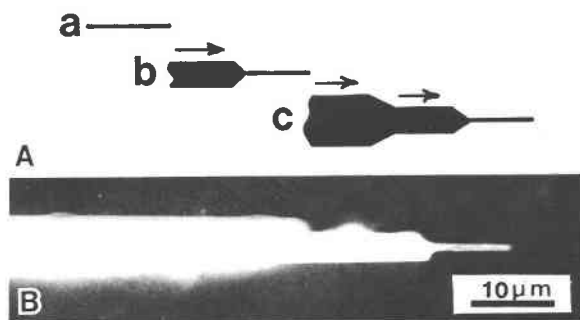


Fig. 3. (A) Stages in whisker growth: (a) leader; (b) and (c) secondary thickening. Modified from Evans (1972). (B) SEM photomicrograph of a typical fiber termination from No. 1 Mansfield 1685.4-1686.0.

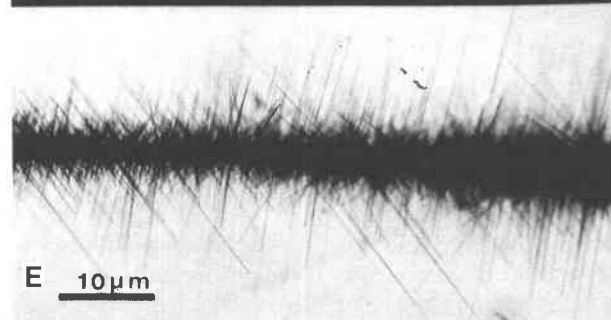
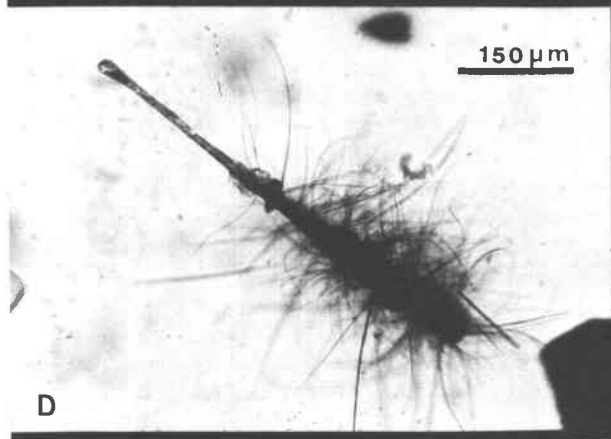
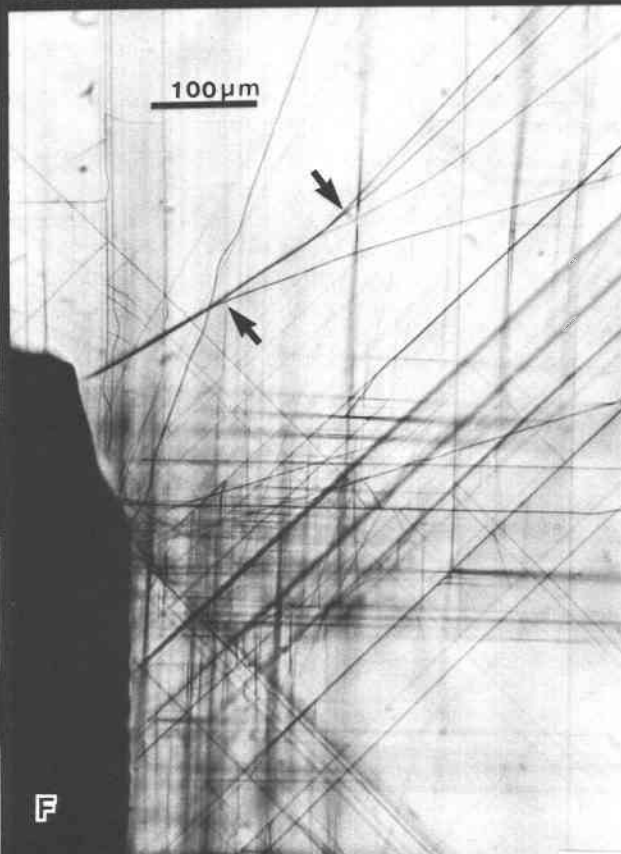
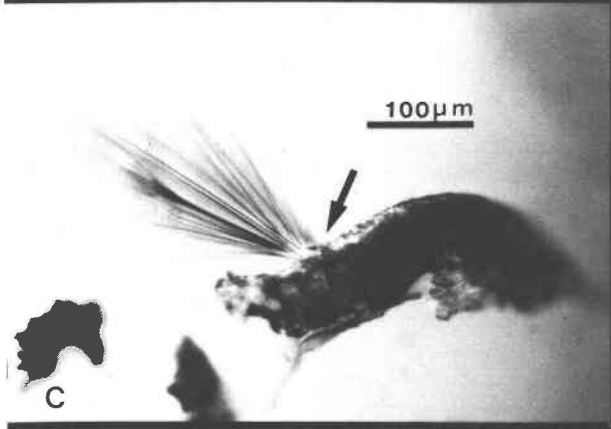
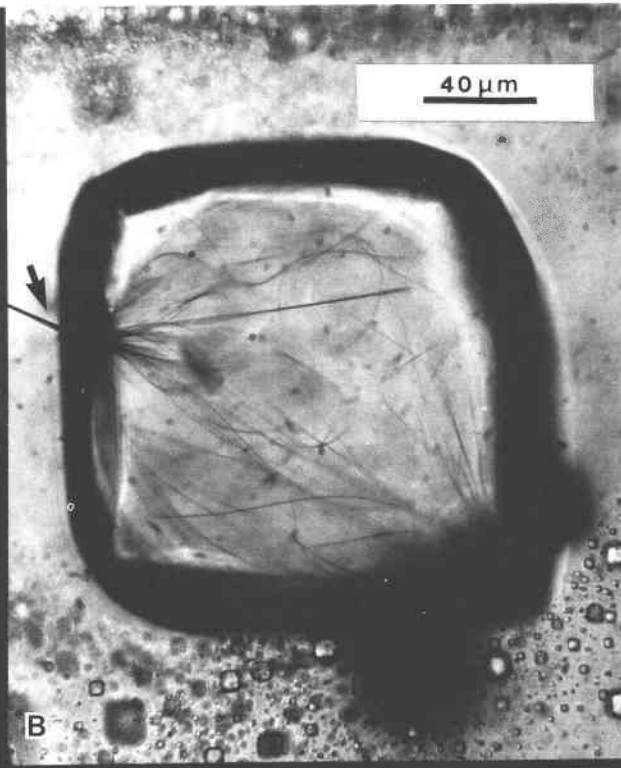
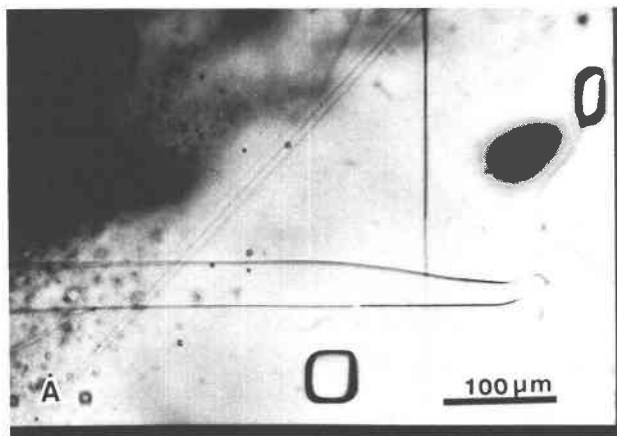
Their thicknesses range from  $< 1$  to  $\sim 10 \mu\text{m}$  as seen with oil-immersion,  $1200\times$ , transmitted light; however, the smaller fibers are difficult to measure. Fiber lengths less than  $\sim 100 \mu\text{m}$  are rare. The longest observed fiber is  $\sim 2$  cm, with an  $\sim 2\text{-}\mu\text{m}$  thickness, yielding an aspect ratio of 10000:1. The fibers can be straight, curved, or both (Figs. 4A, 4F). Straight fibers have been observed to lie commonly along the [100], [110], and [111] directions in the surrounding halite, although they have also been observed in random orientations. Dense areas of fibers often show a grid pattern (Fig. 4F). The straight fibers have been observed in branching and parallel patterns (Figs. 4F, 6D), but most commonly as isolated fibers (Fig. 5B).

Curved fibers, although not as common as the straight fibers, also occur in many different patterns. The curved fibers are found in hairpin patterns (Fig. 4A), in masses of curved fibers (Figs. 4D, 5E), in spirals (Figs. 5C, 5I), and as single isolated curved fibers (Fig. 5B). Straight and curved sections can also occur along the same individual fiber (Fig. 6C).

The terminations of the individual fibers are difficult to observe. SEM studies show that most terminations form a series of tapered steps ending in a thickness of  $\leq 1 \mu\text{m}$  (Figs. 3A, 3B). This is similar to the terminations characteristic of whiskers produced by one-dimensional growth (Evans, 1972). The fibers usually have either square or rectangular cross sections.

### Fiber-fluid inclusion relationship

Although the fibers are most commonly observed as single, isolated individuals in salt, sometimes they are observed in fluid inclusions. The relationship that the fibers have with fluid inclusions is complex although in general the fibers are curved when inside an inclusion. A common feature is that an individual fiber, straight when observed along its length in solid salt, is curved when in a fluid inclusion (Fig. 5E). Inclusion walls also appear to have served as the sites for fiber radiation.



### Fibers radiating from point or line source and in and out of fluid inclusions

One easily recognized feature is fiber radiation: multiple fibers seemingly originating from a common source. This feature was observed in all the cores studied and has a variety of morphologies and patterns.

Radiation from a point source is most common (Fig. 5D). The fibers occur as a single isolated starburst or in clusters (Fig. 5F). Such fibers are often  $>100\ \mu\text{m}$  in length and are usually straight. In only a few cases have we observed radiation from a line source. Figure 4E shows a portion of a line source that was  $\sim 1\ \text{cm}$  long. The fibers are unusually short ( $<100\ \mu\text{m}$ ) and are straight.

Radial fibers are frequently associated with fluid inclusions. Radiation of fibers is observed both into and out of single- or two-phase fluid inclusions as well as from inclusions filled with a mixture of clay, unidentified opaque material, and liquid. The most common pattern observed is the radiation of straight fibers from the inclusion wall (Fig. 4C), although in a few cases curved fibers were observed (Fig. 4D). Figure 4B shows a relatively thick fiber whose intersection with a fluid-inclusion wall is the site of radiation into the inclusion. Similarly, curved fibers in a fluid inclusion when intersecting the inclusion wall serve as the sites for radiation of straight fibers in the solid salt.

In four cases we have observed a fiber seemingly radiating from a fluid inclusion with small inclusions along its length (Figs. 6A, 6B). These fibers are always curved and were seen in clear salt along with inclusions with large vapor bubbles. The small fluid inclusions seem to preferentially wet the fiber (Fig. 6B).

### Fibers and grain boundaries

Fibers have been seen to be completely enclosed within a single crystal of halite or are seen to either stop or cross grain boundaries. Most fibers cross grain boundaries without deviation, although in a few cases (Fig. 5B) fibers were seen to bend upon crossing. In some cases fibers stopped at grain boundaries (Fig. 5A). Such fibers some-

times have thicker ends near the grain boundary, and this appears to be material deposited by grain-boundary fluids.

### Other shapes

Other fiber shapes were observed in a few cases, but only in fluid inclusions in clear salt. Figure 5G shows a blade shape, and Figure 5H shows a thin plate. In one case we observed a blade shape seemingly changing along its length to a fiber that penetrated the inclusion wall (Fig. 7F).

### Fibers in relation to cylinders

Fibers do not have an obvious relationship to cylinders; however, fibers are always found within  $\sim 1\ \text{cm}$  of cylinders, but not the reverse. Fibers are never seen attached to or passing through a cylinder. Fibers can also occur in fluid inclusions with cylinders (Fig. 7K).

### Abundance of fibers

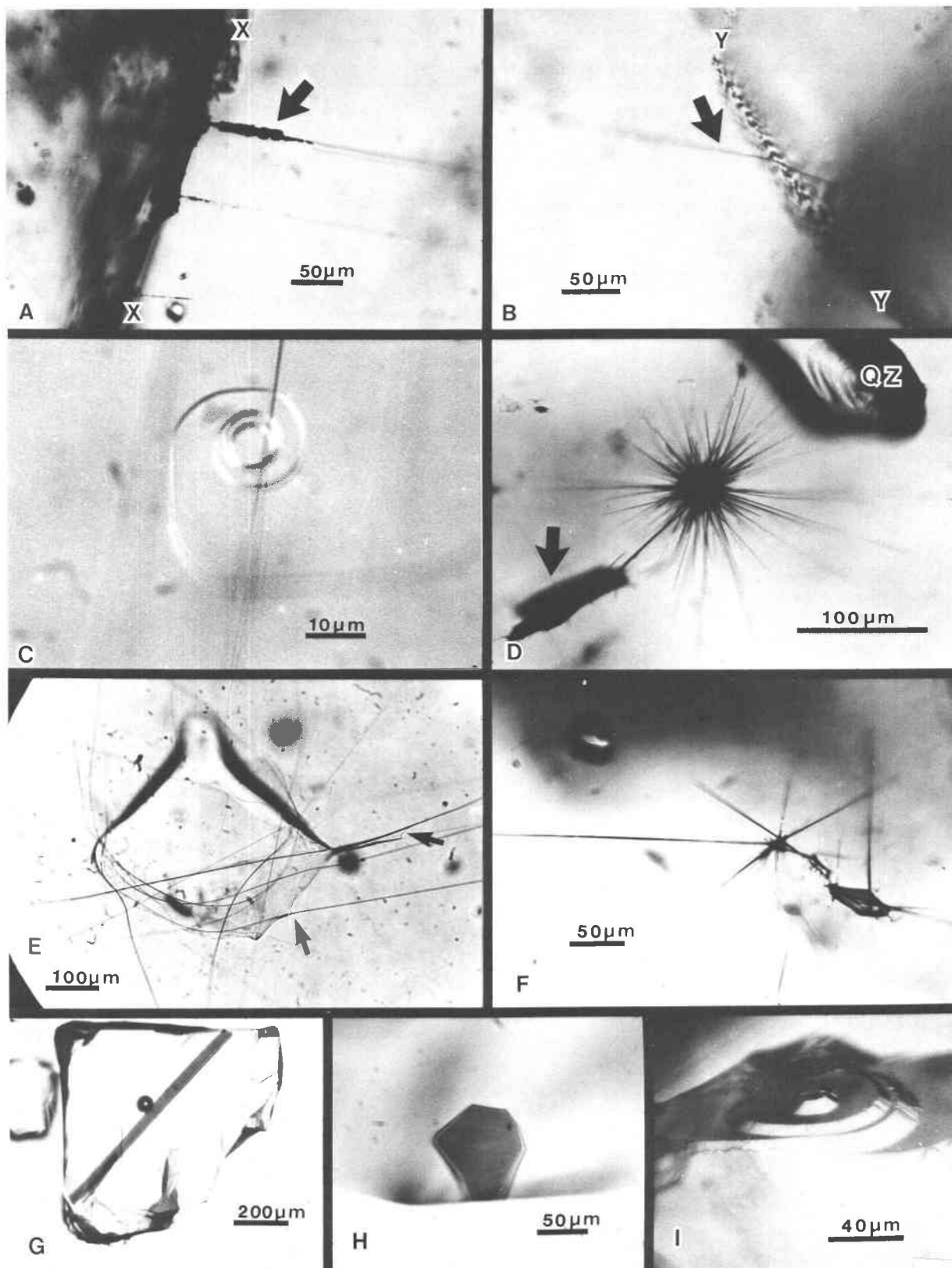
It is difficult to assess the abundance of fibers because of their very irregular distribution. However, an attempt was made to determine the range of concentration by taking representative salt volumes of  $\sim 1\ \text{cm}^3$  and calculating the volume of fibers contained therein. The concentration was found to vary from the ppb to the ppm range. The fibers are more common in the clear salt than in the chevron salt; however, the clear salt is more abundant than the chevron salt.

### Cylinder morphology

A total of 71 cylinders composed of cryptomelane-hollandite have been found in chevron and clear salt in the lower San Andres (units 4 and 5) and the upper San Andres Formations (Table 1). They are smooth, straight, open-ended right cylinders. (Figs. 7A, 7B). The walls are very thin (Figs. 7B, 7M), usually  $\sim 2\ \mu\text{m}$ , although some appear thinner. Within the limits of microscope resolution, they have perfectly circular cross sections, although when they are removed from their fluid-inclusion or halite environment, they deform (Fig. 7M). Figure 8 shows the

---

Fig. 4. (A) Curved and straight fibers from No. 1 Mansfield 1589.7–1590.2. Fibers (slightly out of focus on the left) are continuous from primary chevron salt (left) to clear salt (right). The fibers are  $2\text{--}4\ \mu\text{m}$  in thickness. (B) Primary fluid inclusion in a crystal of clear salt surrounded by chevron salt from No. 1 Mansfield 1622.6–1623.1. This is a clear band within banded (chevron) growth and is presumably original primary growth, as opposed to most “clear salt.” A long ( $>1\ \text{mm}$ ) straight fiber transecting clear and chevron salt “ends” at the inclusion wall (arrow). Numerous straight and curved fibers radiate into the liquid from this point. There are also other groups of fibers radiating from point sources in the inclusion at or near the inclusion wall. (C) Primary inclusion in clear salt from No. 1 J. Friemel 2642.9–2643.2. The inclusion contains fluid and much birefringent and nonbirefringent material. Many ( $>100$ ) straight fibers appear to emanate into the salt from a point on the inclusion wall (arrow). (D) A large flat primary inclusion in clear salt from No. 1 Grabbe 1056.2–1056.8. The inclusion is filled with fluid, birefringent and nonbirefringent material. This view shows the inclusion edge on. Hundreds of fibers emanate into the salt from the inclusion wall; all the fibers are curved; no straight fibers were observed. (E) A long ( $\sim 1\ \text{cm}$ ) fuzzy fiber in clear salt from No. 1 Zeeck 2149.3–2149.7. Thousands of only straight fibers appear to emanate from a line source. This was X-rayed by the Gandolfi technique and proved to be cryptomelane-hollandite. (F) A network of predominantly straight but including some curved fibers adjacent to a large fluid inclusion (dark area resulting from total reflection on the left) in clear salt from No. 1 Mansfield 1685.4–1686.0. This inclusion contains three cylinders. The fibers commonly lie along [100] and [110]. Some branching fibers are also present (arrows).



distribution of all 71 cylinders as a function of length and diameter. The majority are longer than they are wide with a mode of  $\sim 20 \mu\text{m}$  in diameter and variable length. This variability produces a range of shapes from rings (Figs. 7G, 7J, 7K) to straws (Fig. 7C). Rarely they appear to have variable thickness in a pattern parallel to the ends (Fig. 7B). They tend to break parallel to the ends (Fig. 7M). In only one instance did we observe a naturally deformed cylinder (Fig. 7E). This particular cylinder also has very thin walls  $\leq 1 \mu\text{m}$ .

### Cylinders and fluid inclusions

All cylinders are found either in or very near a fluid inclusion (e.g., Figs. 7D, 7L). Some cylinders are found partially in the fluid inclusion and partially in the halite (Fig. 7C). The most striking difference in the cylinder distribution between chevron and clear salt is the occurrence of multiple cylinders in the same fluid inclusion, common in the clear salt but absent in the chevron salt. Also, cylinders completely surrounded by halite or partially out of the fluid inclusion were common in chevron salt but uncommon in clear salt. However, the number that we found—12 cylinders in chevron salt and 59 in clear salt—probably reflects the proportions of chevron to clear salt in our sample rather than any fundamental difference in abundance. Figure 8 shows that the sizes of the cylinders in both chevron or clear salt are similar. Also shown in Figure 8 is a population from an exceptional inclusion in clear salt that contains 14 cylinders; this population is similar in its size distribution to the whole.

The cylinder size and distribution are not related to the characteristics of the host inclusion; therefore, they do not appear to be daughter crystals but were probably accidentally trapped during chevron (e.g., Fig. 7H, 7I) and clear salt (e.g., Fig. 7A) formation.

## DISCUSSION

### Mn in salt

Hauerite ( $\text{MnS}_2$ ) is a common minor constituent in the insoluble residues of bedded salt deposits (Schaller and Henderson, 1932). Taylor (1937) found hauerite as free

or as a cementing material between anhydrite in seven Gulf Coast Louisiana salt domes. Stewart (1963) also reported that hauerite has been found in the water-insoluble residues of the salt domes in Texas. Bein and Land (1983) have determined the Mn content in carbonates from the San Andres Formation. They found a bimodal distribution correlated with Fe content that ranged from 10–50 ppm Mn (low Fe) to 50–450 ppm Mn (high Fe). White et al. (1963) reported 26 ppm Mn in a brine from the Salado Formation, New Mexico, and Stewart (1963) gave a range of 14–390 ppm Mn for various lithologies in the Salado Formation. Schaller and Henderson (1932), in a detailed study of the mineral contents of drill cores from the potash fields of Texas and New Mexico, did not report any cryptomelane-hollandite fibers.

Serdyuchenko (1980) discussed the relationship of some saline basins and their manganese ore contents and stated that some of the upper Paleozoic manganese deposits of the Ural region contain 2 to 8.2 wt% Mn as rhodochrosite, alabandite, and hauerite. These deposits are associated with Lower Permian evaporites with a high Mn content.

Although Mn is just a very minor element in most evaporite deposits, and although we do not have bulk chemical analyses of the formations we studied, it appears very reasonable to assume that there is sufficient Mn in the salt environment to account for the mass of cryptomelane-hollandite fibers and cylinders that we observe. Therefore, it is not necessary to have Mn introduced into the evaporite environment after deposition.

### Organic deposition of Mn

Various Mn compounds are readily precipitated by organisms (e.g., *Metallogenium personatum* and *Pseudomonas manganoxidans*) in both fresh and saline water environments (Crerar et al., 1980; Neilson, 1983; Thiel, 1925; Schweisfurth et al., 1980). Both extant and fossil organisms have been identified with the formation of sedimentary Mn deposits. We found no similarity between the cylinders or fibers and the photographs or drawings of various Mn-precipitating organisms, and we know of no organisms that produce such features. Thus, we conclude that the cylinders and fibers are inorganic.

←  
 Fig. 5. (A) Straight fibers in clear salt from No. 1 Mansfield 1690.8–1691.3. The fibers do not cross a boundary (X–X) between two crystals of clear salt. The ends of the fibers (arrow) are enlarged and opaque. (B) A single fiber in clear salt from No. 1 J. Friemel 2642.9–2643.2. The fiber (arrow) is bent at the boundary (Y–Y) of two clear salt crystals. (C) A spiral fiber in clear salt from No. 1 Mansfield 1638.6–1639.0. There are many straight fibers in the area but out of the plane of focus. (D) A large “star burst” cluster of mostly straight fibers in clear salt from No. 1 J. Friemel 2642.9–2643.2. A crystal of quartz (QZ) is unrelated to the fibers, but an opaque mass (arrow) also has fibers emanating from it. (E) A primary fluid inclusion in clear salt from No. 1 Mansfield 1690.8–1691.3. Most fibers in halite are straight, but curved in the fluid. Note “wetting” of fibers by fluid (arrows). (F) Two fiber “star-bursts” from a cluster of 10 in clear salt from No. 1 J. Friemel 2642.9–2643.2. (G) A large primary fluid inclusion in clear salt from No. 1 Mansfield 1685.4–1686.0. The inclusion contains a large ( $\sim 30 \mu\text{m}$  wide) flat “fiber” as well as other “normal” fibers (out of focus). (H) A primary fluid inclusion in clear salt from No. 1 J. Friemel 2642.9–2643.2. The inclusion contains a six-sided flat piece that appears on the basis of birefringence, color, and pleochroism to be the same material as nearby fibers. (I) The wall of a large primary fluid inclusion in clear salt from No. 1 J. Friemel 2580.7–2581.1. Note the spiral and circular steps that appear to have formed from the movement of the inclusion with a curved fiber in the inclusion wall.

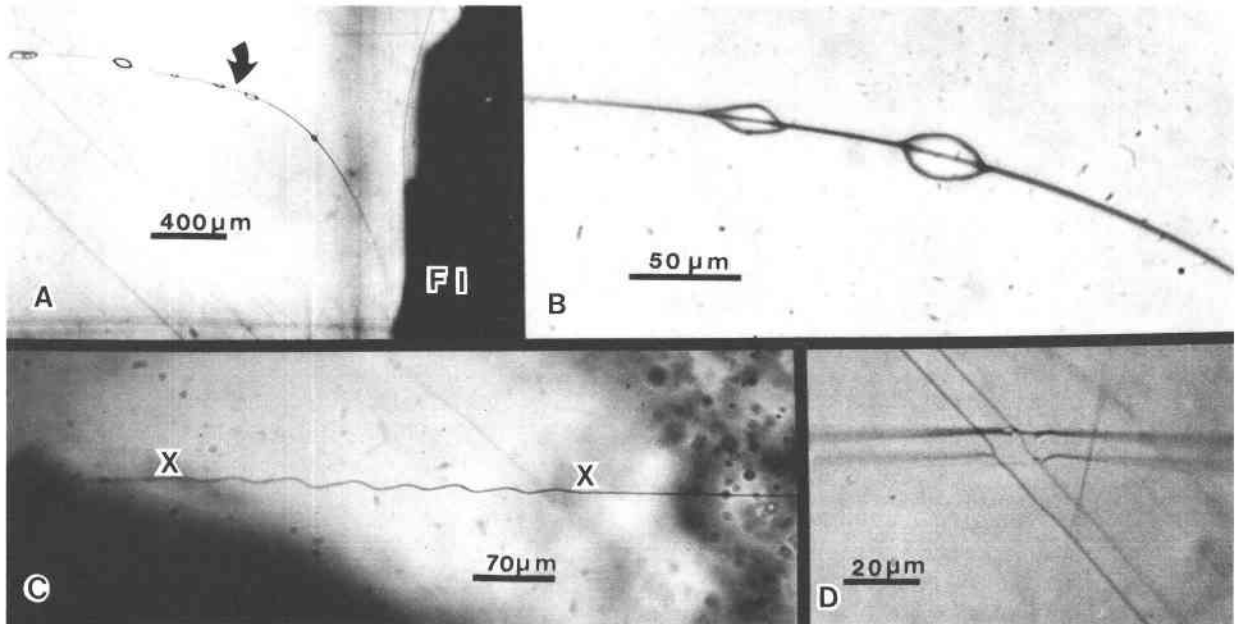


Fig. 6. (A) A curved fiber emanating from a large fluid inclusion (FI) in clear salt from No. 1 Mansfield 1690.8–1691.3. The fiber is the locus for a chain of smaller fluid inclusions (see Fig. 6B). There are many other fibers without these inclusions in the area. (B) Enlargement of the area marked by an arrow in Fig. 6A. Note that the inclusion fluid appears to preferentially wet the fiber. (C) A portion of a fiber (~3 mm long) that transects clear and chevron salt from No. 1 Mansfield 1690.8–1691.3. The fiber shows a wave form (X–X) in one section of its overall length. This wave pattern is common in straight fibers although the wavy portion is usually only ~100 to 200  $\mu\text{m}$  in length. (D) Two pairs of parallel fibers in clear salt from No. 1 Mansfield 1690.8–1691.3. They appear to occupy the same plane at their intersection.

### Origin of the fibers

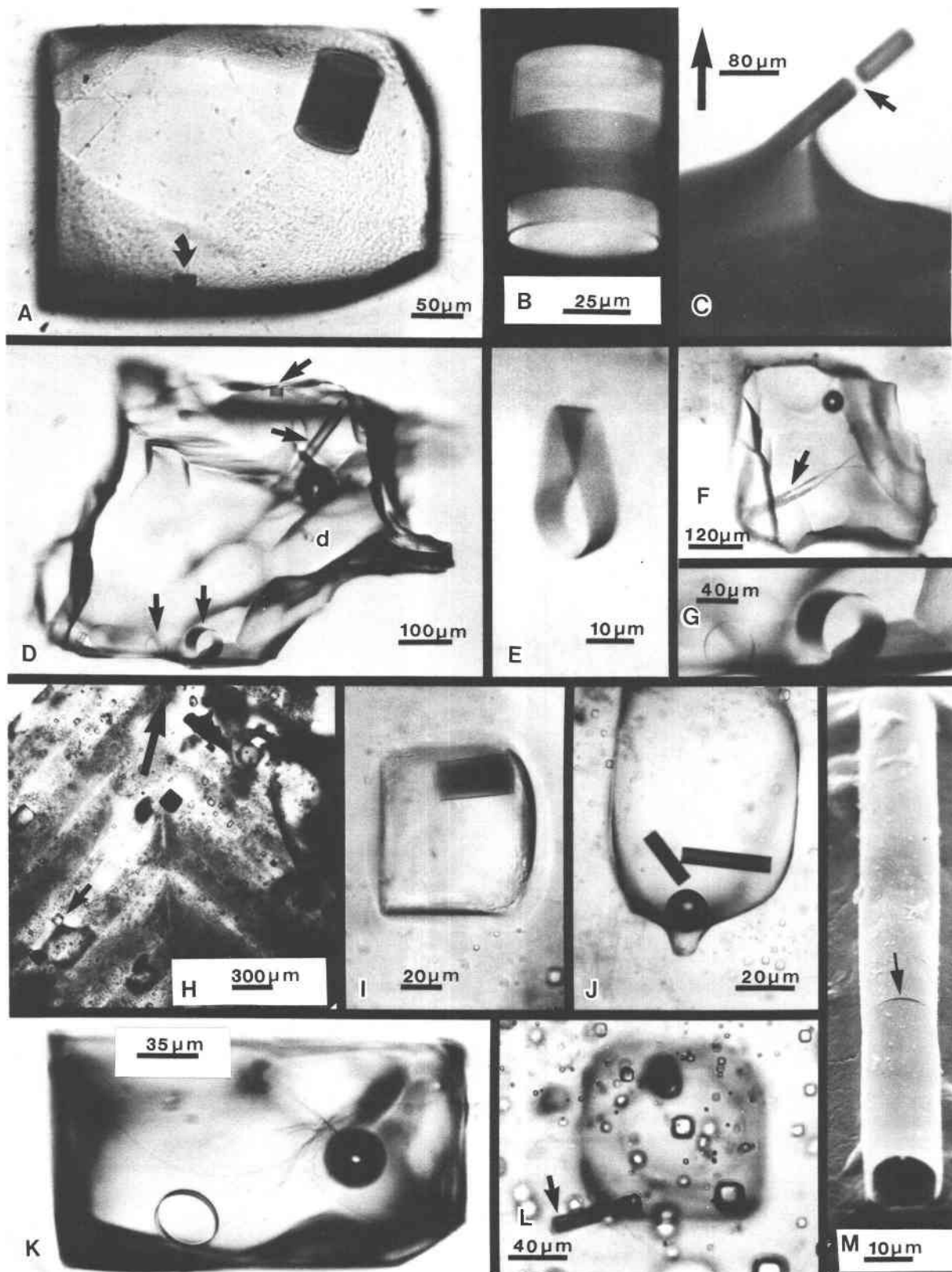
Although the growth mechanism and origin of the cryptomelane-hollandite fibers cannot be determined from the available observations, various observed petrographic features constrain or limit the possibilities.

The fibers are whiskers by the definition of Evans (1972); the characteristic feature of whisker growth is its

one-dimensional nature whereby material is incorporated only at the growing whisker tip. Three general whisker-growth mechanisms have been proposed to explain growth in different environments (Shaffer, 1967): (1) liquid-phase growth (solutions, melts), (2) vapor-phase growth (reaction, sublimation, disproportionation), and (3) growth by solid diffusion.

The fibers are contained in and transect both salt types,

Fig. 7. (A) Large fluid inclusion in clear salt from No. 1 Mansfield 1638.6–1639.0 that contains two cylinders. The axis of rotation of the small cylinder (arrow) is oriented left to right. The fluid inclusion is a negative cube modified by curved faces of the octahedron (pebbly surface). There are eight more cylinders within 5 mm of this inclusion. The inclusion also contains a few fibers (out of focus). (B) An enlargement of the large cylinder in Fig. 7A photographed in crossed nicols. The banding in birefringence is a result of areas of different thickness. (C) Fluid inclusion with cylinder in clear salt from No. 1 J. Friemel 2642.9–2643.2. The large arrow indicates the stratigraphically up direction. This cylinder is the longest one found (~435  $\mu\text{m}$ ). The cylinder is partially in the inclusion and partially enclosed by salt. The small arrow marks a gap in the cylinder. (D) Large fluid inclusion (no. 106 in Fig. 8) in clear salt from No. 1 Mansfield 1690.8–1691.3 that contains 14 regular cylinders (see Fig. 8) and 1 deformed cylinder (see Fig. 7E). The cylinders show a wide variety of sizes. Only four regular cylinders are visible in this plane of focus (arrows). See also Fig. 7G. (E) Enlargement of the deformed cylinder *d* shown in Fig. 7D. (F) Fluid inclusion in clear salt from No. 1 Mansfield 1690.8–1691.3 that has a wide flat fiber that tapers to “normal” thin fibers. (G) Two cylinders seemingly attached to the fluid inclusion wall. This view is an enlargement of Fig. 7D. (H) Small fluid inclusions outlining a chevron structure from No. 1 Mansfield 1690.8–1691.3. The large arrow indicates the stratigraphically up direction. The small arrow marks the fluid inclusion shown in Fig. 7I. (I) Enlargement of the fluid inclusion from Fig. 7H containing one cylinder. (J) Fluid inclusion in clear salt from No. 1 Mansfield 1690.8–1691.3 that contains two cylinders with intermediate length to width ratios. (K) Fluid inclusion in clear salt from No. 1 Mansfield 1685.4–1686.0 that contains one cylinder and many fibers. This cylinder is typical of those with a low length to width ratio. (L) A group of small inclusions in chevron salt from No. 1 Mansfield 1690.8–1691.3. The cylinder (arrow) is completely surrounded by salt. The large fluid inclusion, just out of focus, is stratigraphically below the hollow cylinder. (M) A SEM photomicrograph of a cylinder from clear salt from No. 1 Mansfield 1690.8–1691.3. The cylinder has been removed from a fluid inclusion



and washed out on a halite cleavage surface and has been slightly deformed. Energy-dispersive analysis of this cylinder showed major Mn with moderate K and minor Ba. Note the crack (arrow) that occurred during the washing procedure.

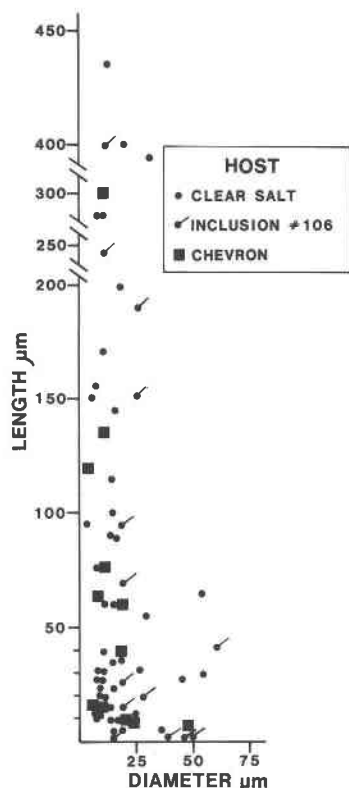


Fig. 8. A plot of the dimensions of the 71 cylinders found in clear and chevron salt. The length is measured parallel to the axis of rotation and the diameter perpendicular to it. The 14 cylinders found in inclusion no. 106 (Fig. 7D) are distinguished from the others found in clear salt.

chevron and clear salt. We see no evidence that solution, recrystallization, or deformation has occurred after fiber growth (at least in proximity to the fibers). Thus, we conclude that the fibers are postsalt. The numerous examples of radial growth from a point, line or planar surface suggest a directional growth process involving the addition of material at the fiber tip. The solid-state diffusion processes associated with whisker growth are not very well understood (Evans, 1972). Most cases have been studied at temperatures near the melting point of the host. The petrography and chemistry of the fibers also appear to preclude precipitation phenomena such as Suzuki phases (Guerrero et al., 1980; Bhagavan Raju et al., 1980) or exsolution.

Two features of the salt and fibers may have aided in a diffusional growth process. First, dislocations are common in natural salt (Shlichta, 1968), and diffusion along these dislocations may have been a significant process (Tucker et al., 1963; Fredericks, 1975). Second, cryptomelane-hollandite has a structure containing parallel, open tunnels of ionic size (Turner and Buseck, 1979). Huggins (1975) suggested that such materials may have rapid ionic transport in the tunnel direction. TEM studies would be valuable to determine the orientation of the structure relative to fiber elongation.

Although fluid inclusions cannot be genetically related to the fibers, there are some features (Fig. 4B) that suggest involvement of inclusion fluid in fiber growth. Fiber radiation into fluid inclusions indicates that some fibers grew in a liquid environment. Nevertheless, we tentatively propose that fiber growth in the salt may have been a solid-state diffusion process occurring at low temperatures.

#### Origin of the cylinders

Although both the cylinders and the fibers appear to be composed of cryptomelane-hollandite, they do not seem to be related in origin. The cylinders seem to occur as accidentally trapped objects in both the chevron and the clear salt. The fibers formed after the salt whereas the cylinders appear to have been present during the primary and subsequent salt crystallization.

Cylinders and/or rings have been infrequently reported in the mineralogical literature. Bates et al. (1950) suggested that cylinders ( $\sim 400\text{-\AA}$  diameter) of endellite are created by a mismatch between the interlayered kaolinitic and water layers. Similar cylinders ( $\sim 110\text{-\AA}$  diameter) of chrysotile (Bragg and Claringbull, 1965) are formed the same way. The degree of mismatch determines the radius of curvature. If the cryptomelane-hollandite cylinders are formed this way, then the degree of mismatch is slight relative to that of halloysite or chrysotile. Bideaux (1970) described a variety of mineral species that occur as rings or cylinders. Most similar in appearance to the cryptomelane-hollandite cylinders are cylinders of jamesonite (Bideaux, 1970; Fig. 4) and of rutile in topaz (Bideaux, 1970; Fig. 10). Fibers of the same cylinder material are also found in the same host environment. Bideaux (1970) suggested two mechanisms for cylinder formation: (1) epitaxial growth and (2) circular growth by surface-tension wrapping around an immiscible droplet. These two mechanisms do not seem appropriate for the cryptomelane-hollandite cylinders.

There is a difference in the observed cylinder distribution between chevron and clear salt. Only one cylinder per fluid inclusion is found in the chevron salt whereas multiple cylinders are commonly found in inclusions in clear salt. The common multiple cylinders in the clear salt may reflect a concentration process that occurred during dissolution and recrystallization of the primary chevron salt. Cylinders trapped in chevron salt would perhaps remain as a residue after salt dissolution and might be trapped in the less common but much larger fluid inclusions characteristic of the clear salt (Roedder, 1984). However, this process would have to be exceedingly gentle to preserve the relatively fragile cylinders.

Although our observations have not allowed determination of the origin of the cylinders, we believe that they are a primary feature of salt crystallization.

#### Natural migration of fluid inclusions

A common feature of cylinders in chevron and clear salt is their occurrence partially out of their host fluid inclusion (Figs. 7C, 7L) or completely in salt but near a

fluid inclusion. Two important features that are observed are (1) these salt-hosted cylinders are usually near large inclusions ( $> 10^6 \mu\text{m}^3$ ) and (2) they occur *above* the inclusion, in the stratigraphic sense, suggesting that the inclusions may have moved downward, leaving the cylinders behind. Roedder (1984) and Roedder and Belkin (1980) have discussed the laboratory and natural migration of fluid inclusions in salt by dissolution and reprecipitation in thermal gradients. Roedder (1984) has pointed out that the delicate patterns of small fluid inclusions that outline the chevron salt have remained intact after formation even though they have been in the geothermal gradient for hundreds of millions of years. Indeed, in the salt that we studied, the small-inclusion patterns seem to have remained intact. However, larger inclusions were found to move much more rapidly than small ones, possibly explaining the cylinder-inclusion separation noted here. Also, our observation of inclusion-free volumes above certain large inclusions ( $\geq 60 \mu\text{m}$  on an edge) suggests that they migrated downward (1–3 inclusion-edge lengths in distance), removing by coalescence the inclusions in their path. Thus, these two observations indicate that some natural fluid-inclusion migration has occurred in this environment.

In only four cases did we observe fluid inclusions along a fiber (Figs. 6A, 6B). This suggests that some fluid movement has occurred along some fibers. Furthermore, the formation of the fibers after salt crystallization or recrystallization and the recognition of some natural fluid-inclusion migration suggest that at some stage in their history, various mass-transport processes were operative in these rocks.

### CONCLUSIONS

Mineralogical curiosities often lead to important advances in the understanding of mineral or rock paragenesis. Fibers and cylinders should be looked for in other bedded-salt environments. Further petrographic, chemical, and especially electron-microscope studies should help to more closely identify their origin.

In summary, (1) The fibers and cylinders occur in both the chevron and clear salt. (2) Their composition is the cryptomelane-hollandite series with variable K and Ba substitution. (3) The cylinders appear to have been accidentally trapped in fluid inclusions during primary deposition and subsequent salt recrystallization. (4) The fibers occur in and transect both the chevron and clear salt; thus, they appear to have formed after all salt crystallization. (5) The presence of cylinders extending partially or completely out of the tops of large fluid inclusions suggests that some degree of natural downward fluid-inclusion migration has occurred.

### ACKNOWLEDGMENTS

We gratefully acknowledge the careful reviews of Edwin Roedder (USGS), Howard T. Evans, Jr., (USGS), and Jeffrey E. Post (Smithsonian Institution). We also thank Susan D. Hovorka (Bureau of Economic Geology, The University of Texas at Austin) for her interest and helpful comments.

### REFERENCES CITED

- Ahmad, I. (1970) Growth process of inorganic whiskers. Technical report WVT-7060, Benet R&E Laboratories, Watervliet Arsenal, New York, 117 p.
- Arthurton, R.S. (1973) Experimentally produced halite compared with Triassic layered halite-rock from Cheshire, England. *Sedimentology*, 20, 145–160.
- Bates, T.F., Hildebrand, F.A., and Swineford, A. (1950) Morphology and structure of endellite and halloysite. *American Mineralogist*, 35, 463–484.
- Bein, A., and Land, L.S. (1983) Carbonate sedimentation and diagenesis associated with Mg-Ca-chloride brines: The Permian San Andres Formation in the Texas Panhandle. *Journal of Sedimentary Petrology*, 53, 243–260.
- Bhagavan Raju, I.V.K., Strecker, H., and Strunk, H. (1980) Transmission electron microscopy of doped NaCl crystals. *Journal de Physique*, 41-C6, 376–379.
- Bideaux, R.A. (1970) Mineral rings and cylinders. *Mineralogical Record*, 1, 105–112.
- Bragg, L., and Claringbull, G.F. (1965) Crystal structures of minerals. G. Bell and Sons, Ltd., London, 409 p.
- Crerar, D.A., Fischer, A.G., and Plaza, C.L. (1980) Metallogenium and biogenic deposition of manganese from Precambrian to Recent time. In I.M. Varentsov and Gy. Grasselly, Eds., *Geology and geochemistry of manganese*, vol. III, Manganese on the bottom of recent basins, p. 285–303. E. Schweizerbart'sche Verlagsbuchhandlung, Stuttgart.
- Dutton, S.P., Finley, R.J., Galloway, W.E., Gustavson, T.C., Handford, C.R., and Presley, M.W. (1979) Geology and geohydrology of the Palo Duro Basin, Texas Panhandle, a report on the progress of nuclear waste isolation feasibility studies (1978). Geological Circular 79-1 Bureau of Economic Geology, University of Texas, 99 p.
- Evans, C.C. (1972) Whiskers. Mills and Boon Limited, London, 72 p.
- Finkelman, R.B., Evans, H.T., Jr., and Matzko, J.J. (1974) Manganese minerals in geodes from Chihuahua, Mexico. *Mineralogical Magazine*, 39, 549–558.
- Fleischer, M. (1983) Glossary of mineral species 1983. *Mineralogical Record*, Tucson, 202 p.
- Fleischer, M., and Richmond, W.E. (1943) The manganese oxide minerals: A preliminary report. *Economic Geology*, 38, 269–286.
- Fracasso, M.A., and Hovorka, S.D. (1986) Cyclicity in the Middle Permian San Andres Formation, Palo Duro Basin, Texas Panhandle. Bureau of Economic Geology, University of Texas at Austin, Report of Investigations No. 156, 48 p.
- Fredericks, W.J. (1975) Diffusion in alkali halides. In A.S. Nowick and J.J. Burton, Eds., *Diffusion in solids, recent developments*, p. 381–444. Academic Press, New York.
- Frenzel, G. (1980) The manganese ore minerals. In I.M. Varentsov and Gy. Grasselly, Eds., *Geology and geochemistry of manganese*, vol. I, General problems, p. 25–157. E. Schweizerbart'sche Verlagsbuchhandlung, Stuttgart.
- Gandolfi, G. (1967) Discussion upon methods to obtain X-ray "powder patterns" from a single crystal. *Mineralogica et Petrographica Acta*, 13, 67–74.
- Guerrero, A.L., Butler, E.P., and Pratt, P.L. (1980) The Suzuki phase in NaCl: Cd<sup>2+</sup> and NaCl: Mg<sup>2+</sup>. *Journal de Physique*, 41-C6, 363–366.
- Handford, C.R. (1981) Coastal sabkha and salt pan deposition of the lower Clear Fork Formation (Permian), Texas. *Journal of Sedimentary Petrology*, 51, 761–778.
- Hewett, D.F., and Fleischer, M. (1960) Deposits of manganese oxides. *Economic Geology*, 55, 1–51.
- Hovorka, S.D. (1983) Carbonate-anhydrite-halite cycles, San Andres formation (Permian) Palo Duro Basin, Texas. In R.L. Shaw and B.J. Pollan, Eds., *Permian Basin cores—A workshop*, p. 197–224. Society of Economic Paleontologists and Mineralogists, Tulsa, Oklahoma.
- (1985) Model for deposition of bedded halite in a shallow shelf setting, San Andres Formation, Palo Duro Basin, Texas Panhandle. *Geological Society of America Abstracts with Programs*, 17, 614.
- Huggins, R.A. (1975) Very rapid ionic transport in solids. In A.S. Nowick and J.J. Burton, Eds., *Diffusion in solids, recent developments*, p. 445–486. Academic Press, New York.
- Johnson, K.S., and Gonzalus, A. (1978) Salt deposits in the United States

- and regional geologic characteristics important for storage of radioactive waste. Union Carbide, Inc., Oak Ridge, Tennessee, Report Y/OWI/SUB-7414/1, 73 p.
- Kerr, P.F. (1959) Optical mineralogy (3rd edition), McGraw-Hill, New York, 442 p.
- McClain, W.C., and Russell, J.E. (1980) Radioactive waste isolation. In A.H. Coogan and L. Hauber, Eds., Fifth symposium on salt, vol. 2, p. 61–68. Northern Ohio Geological Society, Inc., Cleveland, Ohio.
- Neelson, K.H. (1983) The microbial manganese cycle. In W.E. Krumbein, Ed., Microbial geochemistry, p. 191–221. Blackwell Scientific Publications, Oxford.
- Post, J.E., Von Dreele, R.B., and Buseck, P.R. (1982) Symmetry and cation displacements in hollandite: Structure refinements of hollandite, cryptomelane and priderite. *Acta Crystallographica*, B38, 1056–1065.
- Potter, R.M., and Rossman, G.R. (1979) Mineralogy of manganese dendrites and coatings. *American Mineralogist*, 64, 1219–1226.
- Presley, M.W. (1980) Upper Permian salt-bearing stratigraphic units. Texas Bureau of Economic Geology Geological Circular 80-7, 12–23.
- Radcliffe, D. (1974) Genesis of hypogene psilomelane fibers from the Tower Mines area, New Mexico. *American Mineralogist*, 59, 206–207.
- Richmond, W.E., and Fleischer, M. (1942) Cryptomelane, a new name for the commonest of the "psilomelane" minerals. *American Mineralogist*, 27, 607–610.
- Roedder, E. (1982) Possible Permian diurnal periodicity in NaCl precipitation, Palo Duro Basin, Texas. Texas Bureau of Economic Geology Geological Circular 82-7, 101–104.
- (1984) The fluids in salt. *American Mineralogist*, 69, 413–439.
- Roedder, E., and Bassett, R.L. (1981) Problems in determination of the water content of rock-salt samples and its significance in nuclear waste storage siting. *Geology*, 9, 525–530.
- Roedder, E., and Belkin, H.E. (1980) Thermal gradient migration of fluid inclusions in single crystals of salt from the Waste Isolation Pilot Plant site (WIPP). In C.J.M. Northrup, Ed., Scientific basis for nuclear waste management, vol. 2, p. 453–464. Plenum Press, New York.
- Roedder, E., d'Angelo, W.M., Dorrzapf, A.F., Jr., and Aruscavage, P.J. (1987) Composition of fluid inclusions in Permian salt beds, Palo Duro Basin, Texas. *Chemical Geology*, 61, 79–90.
- Schaller, W.T., and Henderson, E.P. (1932) Mineralogy of drill cores from the potash field of New Mexico and Texas. U.S. Geological Survey Bulletin 833, 124 p.
- Schmalz, R.F. (1969) Deep-water evaporite deposition: A genetic model. *American Association of Petroleum Geologists Bulletin*, 53, 798–823.
- Schweisfurth, R., Jung, W., and Gundlach, H. (1980) Manganese-oxidizing micro-organisms and their importance for the genesis of manganese ore deposits. In I.M. Varentsov and Gy. Grasselly, Eds., *Geology and geochemistry of manganese*, vol. III, Manganese on the bottom of recent basins, p. 279–283. E. Schweizerbart'sche Verlagsbuchhandlung, Stuttgart.
- Serdyuchenko, D.P. (1980) Precambrian biogenic-sedimentary manganese deposits. In I.M. Varentsov and Gy. Grasselly, Eds., *Geology and geochemistry of manganese*, vol. II, Manganese deposits on continents, p. 61–85. E. Schweizerbart'sche Verlagsbuchhandlung, Stuttgart.
- Shaffer, P.T.B. (1967) Whiskers—Their growth and properties. In L.J. Broutman and R.H. Krock, Eds., *Modern composite materials*, p. 197–216. Addison-Wesley, Reading, Massachusetts.
- Shearman, D.J. (1978) Evaporites of coastal sabkhas; ancient sabkha deposits; and halite in sabkha environments; section 2. In W.E. Dean and B.C. Schreiber, Eds., *Marine evaporites*, p. 6–42. Society of Exploration Paleontologists and Mineralogists Short Course Notes No. 4.
- Shlichta, P.J. (1968) Growth, deformation, and defect structure of salt crystals. *Geological Society of America Special Paper* 88, 597–617.
- Stewart, F.H. (1963) Marine evaporites. U.S. Geological Survey Professional Paper 440-Y, 53 p.
- Sun, M.-S. (1962) Oriented growths of cryptomelane in sylvite, Carlsbad, New Mexico. *American Mineralogist*, 47, 152–155.
- Taylor, R.E. (1937) Water-insoluble residues in rock salt of Louisiana salt plugs. *American Association of Petroleum Geologists Bulletin*, 21, 1268–1310.
- Thiel, G.A. (1925) Manganese precipitated by microorganisms. *Economic Geology*, 20, 301–310.
- Tucker, R., Laskar, A., and Thomson, R. (1963) Pipe diffusion in LiF. *Journal of Applied Physics*, 34, 445–452.
- Turner, S., and Buseck, P.R. (1979) Manganese oxide tunnel structures and their intergrowths. *Science*, 203, 456–458.
- White, D.E., Hem, J.D., and Waring, G.A. (1963) Chemical composition of subsurface waters. U.S. Geological Professional Paper 440-F, 67 p.
- Zolensky, M.E., and Bodnar, R.J. (1982) Identification of fluid inclusion daughter minerals using Gandolfi X-ray techniques. *American Mineralogist*, 67, 137–141.

MANUSCRIPT RECEIVED MARCH 24, 1987

MANUSCRIPT ACCEPTED JULY 2, 1987